Synthesis, Structure, Electronic State, and Luminescent Properties of Novel Blue-Light-Emitting Aryl-Substituted 9,9-Di(4-(di-p-tolyl)aminophenyl)fluorenes

ARTICLE *in* ADVANCED FUNCTIONAL MATERIALS · AUGUST 2008

Impact Factor: 11.81 · DOI: 10.1002/adfm.200800075

9 AUTHORS, INCLUDING:

Yi Liao
Capital Normal University
44 PUBLICATIONS **830** CITATIONS
SEE PROFILE

Xinjun Xu
University of Science and Technology Beijing
70 PUBLICATIONS **1,363** CITATIONS
SEE PROFILE

Shanghui Ye
Chinese Academy of Sciences
52 PUBLICATIONS **892** CITATIONS
SEE PROFILE

Yunqi Liu
Albemarle
382 PUBLICATIONS **16,120** CITATIONS
SEE PROFILE

ADVANCED FUNCTIONAL MATERIALS

FULL PAPER

DOI: 10.1002/adfm.200800075

Synthesis, Structure, Electronic State, and Luminescent Properties of Novel Blue-Light-Emitting Aryl-Substituted 9,9-Di(4-(di-*p*-tolyl)aminophenyl)fluorenes**

By *Shibo Jiao, Yi Liao, Xinjun Xu, Liping Wang, Gui Yu,* Limin Wang, Zhongmin Su,* Shanghui Ye,* and *Yunqi Liu**

Novel blue-light-emitting fluorene derivatives **5a–c** and **7a–c** containing bulky and highly emissive groups, namely pyrene, 10-phenylanthracene-9-yl and 10-(4′-diphenylaminophenyl)anthracene-9-yl groups, as well as hole-injecting/transporting triarylamines were synthesized. Single crystals of compounds **5a**, **5c**, **7a**, and **7c** were grown and their crystal structures were determined by X-ray diffraction. The four fluorene derivatives have nonplanar molecular structures, which reduce the intermolecular interaction and the likelihood of molecular aggregation or excimer formation. No unwanted long-wavelength emission was observed in the photoluminescence (PL) spectra of the **5a–c** and **7a–c** thin films. Their PL spectra reveal excellent thermal stability after annealing treatment under air and ambient light. All of the six compounds show high fluorescence quantum yields and outstanding thermal stabilities. The 2-aryl and 2,7-diaryl substituents at the fluorene molecule have a significant effect on the photophysical properties and the thermal characteristics. The six compounds show almost the same energy levels for the highest occupied molecular orbitals (HOMOs) of about −5.20 eV, which allows effective hole injection. The C2- and C7-aryl substituents play a relatively less-important role in the HOMO energy levels, which depend mainly on the triphenylamino groups at the C9 position. The molecular orbitals, excitation energy, and emission energy were calculated to explain the real origin of their photophysical characteristics. The HOMOs are mainly localized on the triphenylamino groups at the C9 position, while the lowest unoccupied molecular orbitals (LUMOs) have a significant orbital density at the C2- and/or C7-aryl substituents. Pure-blue-light-emitting diodes based on 2,7-diaryl-9,9-di(triarylamino)fluorenes were fabricated.

1. Introduction

Since the development of organic light-emitting diodes (OLEDs) by Tang and VanSlyke,[1] organic electroluminescent (EL) materials have attracted significant attention due to their promising applications in full-color flat-panel displays and solid-state lighting.[2–4] During the past decades, great efforts were focused on the development of novel EL materials with intense luminescent efficiency, good thermal/optical stability, excellent charge-carrier injection and transport, and desirable film morphology, as well as on fabrication of high-performance devices.[5–7] Outstanding red-, green-, and blue-emitting materials and devices are necessary to achieve full-color display applications. However, compared with green-light-emitting devices, the EL properties of blue-emitting ones need to be improved, particularly in terms of efficiency and color purity, for full-color applications. Excellent blue-emitting materials are important, not only as blue emitters, but also as hosts for dopant emitters to facilitate efficient green and red emission.[8,9] It is thus important to develop high-performance blue-light-emitting materials with good stability and high fluorescent efficiency. Maintaining efficient carrier injection in the light-emitting device is considered to be a significant issue for achieving high device performance. Unfortunately, the wide energy gaps essential for blue emission often result in a high ionization potential and a low electron affinity (EA), making it difficult to inject both holes and electrons efficiently into blue emitters from the two opposite electrodes in OLEDs, which thus leads to a poor device performance in current blue OLEDs. Efficient electron injection can be achieved by using low-work-function

[*] Prof. Dr. G. Yu, Prof. Dr. Y. Q. Liu, S. B. Jiao, Dr. X. J. Xu, L. M. Wang, S. H. Ye
Beijing National Laboratory for Molecular Sciences,
Institute of Chemistry, Chinese
Academy of Sciences
Beijing 100190, (PR China)
E-mail: yugui@mail.iccas.ac.cn; liuyq@mail.iccas.ac.cn
Prof. Z. M. Su, Dr. Y. Liao
Institute of Functional Material Chemistry,
Faculty of Chemistry, Northeast Normal University
Changchun 130024, (PR China)
E-mail: suyz@nenu.edu.cn
S. B. Jiao, Dr. L. P. Wang, and L. M. Wang
Department of Physics and Chemistry,
School of Materials Science and Engineering,
University of Science and Technology Beijing
Beijing 100083, (PR China)

[**] This work was supported by the Major State Basic Research Development Program, the National Natural Science Foundations of China (20573115, 90206049, 20472089, 20773012), and the Chinese Academy of Sciences. Supporting Information is available online from Wiley InterScience or from the author.

cathodes. Introducing strong electron-withdrawing groups into organic molecules can enhance the EA values, resulting in efficient electron injection.[10] Nevertheless, application of blue-emitting acceptors as an emissive layer in OLEDs is very limited due to the formation of exciplexes with the electron-donating arylamine compounds, which are widely used as the hole-transporting material.[11] Doping of the blue-emitting molecules into a wide-band-gap host material is one of the most-effective approaches to enhance hole injection and reduce concentration quenching in emitters. This approach suffers from the obvious problem of phase separation occurring over time with consequent device instability. Using an additional hole-injection/transporting layer could also compensate for poor hole injection. However, these approaches are subject to a complicated fabrication process. Consequently, it is essential to synthesize blue-emitting materials with a high energy level of the highest occupied molecular orbitals (HOMOs), facilitating both hole injection and transport.

Searching for new blue-emitting materials with high-performance remains one of the major challenges, although a large number of EL materials have been synthesized and investigated.[12] Among the blue-emitting materials, fluorenes, spirofluorenes, oligomeric fluorenes, polyfluorenes (PFs), and their derivatives are regarded as the most promising candidates for blue OLEDs.[13–15] They exhibit high fluorescent efficiencies, thermal stability, and good solubility. However, fluorene derivatives show an unwanted long-wavelength emission that is attributed to aggregation, excimer emission, or fluorenone defects.[16] The photo- or electro-oxidized cleavage of C9-substituted alkyl group(s) also results in long-wavelength emission.[17] To avoid emissive fluorenone defects formed by oxidation of monoalkylfluorene impurities, Holmes developed full 9,9-diakylkylated PFs, which suppress the emission attributed to ketone defects in photoluminescence and electroluminescence.[18] Replacing a C9 carbon of the PFs with silicon was used to prevent the fluorenone defect.[19] Introduction of bulky groups at the C9 position of the fluorene to suppress formation of the aggregation or excimer in order to obtain stable blue emission was attempted.[20] Another drawback of fluorene derivatives is the low HOMO energy level, which leads to inefficient hole injection. Highly electron-rich triphenylamines known for their high hole mobility have been extensively used as the hole-transporting material in OLEDs. The advantage of the incorporation of triphenylamino groups is that they can increase the HOMO energy levels, reducing the energy barrier for hole injection from the indium tin oxide (ITO) to the emissive layer.[21] Wong reported blue-light-emitting 9,9-diarylfluorene-based triaryldiamines, which exhibit low emission quantum yields.[22] In previous work, we reported 9,9-bis(triarylamino)-substituted fluorenes that exhibit high HOMO energy levels from −5.0 to −5.3 eV. Unfortunately, we were not able to obtain blue OLEDs based on these materials due to the formation of electromers.[23]

In OLED devices, organic materials are practically utilized as thin films. Therefore, high photoluminescence (PL) quantum yields in the solid state are essential to obtain efficient electroluminescence. Most organic light-emitting materials have a high quantum efficiency in solution, whereas they become weakly luminescent in thin films. In the solid state, the molecules aggregate to form less-emissive species such as excimers, resulting in low luminescence efficiency. Molecules with both the three-dimensional nonplanar conformation and the certain conjugation degree can exhibit high luminescence efficiency in the solid state.[24] These nonplanar structures are helpful in preventing the formation of excimers and in reducing aggregation PL quenching in the solid state.

In this work, we have designed and synthesized novel blue-light-emitting 2-aryl-9,9-di(triarylamino)fluorenes and 2,7-diaryl-9,9-di(triarylamino)fluorenes. These fluorene derivatives contain bulky and highly emissive groups, namely pyrene, 10-phenylanthracene-9-yl, or 10-(4′-diphenylaminophenyl) anthracene-9-yl groups, which can increase the fluorescence quantum yield. Introducing hole-injection/transporting triarylamines into the C9 position of the fluorene is beneficial for improving the HOMO energy levels of the fluorene derivatives. Attachment of bulky substituents at the C2 and C9 positions is advantageous in enhancing the thermal stability. The fluorene derivatives exhibit three-dimensionally noncoplanar structures, which effectively inhibit self-aggregation and/or the excimer formation in the solid state. Thin films of the fluorene derivatives show a blue emission with a peak at 440–470 nm without any tail in the longer-wavelength region, while their PL spectra reveal an excellent thermal stability upon air annealing. These new compounds can serve as excellent emitting materials for blue OLEDs, emitting blue light with stable Commision Internationale de l'Eclairage (CIE) coordinates under different driving voltages.

2. Results and Discussion

2.1. Synthesis of 9,9-Di(4-(di-p-tolyl)aminophenyl)fluorene Derivatives

The synthetic routes of the novel blue light-emitting materials are shown in Scheme 1. 9,9-Di[4-(di-*p*-tolyl)aminophenyl]fluorene (**1a**) was synthesized by the reaction of fluorenone and 4,4′-dimethyltriphenylamine in the presence of methanesulfonic acid. Compounds **1b** and **1c** were obtained in a similar way. The lithiation of 4-bromotriphenylamine with an excess amount of *n*-butyl lithium (*n*-BuLi) at −78 °C, followed by treatment with 2-isopropoxy-4,4,5,5-tetramethyl-[1,3,2]dioxaborolane, gave the boronic ester **2**. The Pd-catalyzed Suzuki coupling reaction of the boronic ester **2** with 9,10-dibromoanthracene was accomplished by using a catalytic amount of Aliquat 336 as a promoter to afford 4-(10-bromoanthracene-9-yl)triphenylamine (**3c**) in an 84% yield. Transformation of the bromides **3a–c** into the corresponding pinacolato boronic esters **4a–c** was carried out in the presence of an excess amount of *n*-BuLi at −78 °C followed by treatment with 2-isopropoxy-4,4,5,5-tetramethyl-[1,3,2]dioxaborolane to

ADVANCED FUNCTIONAL MATERIALS

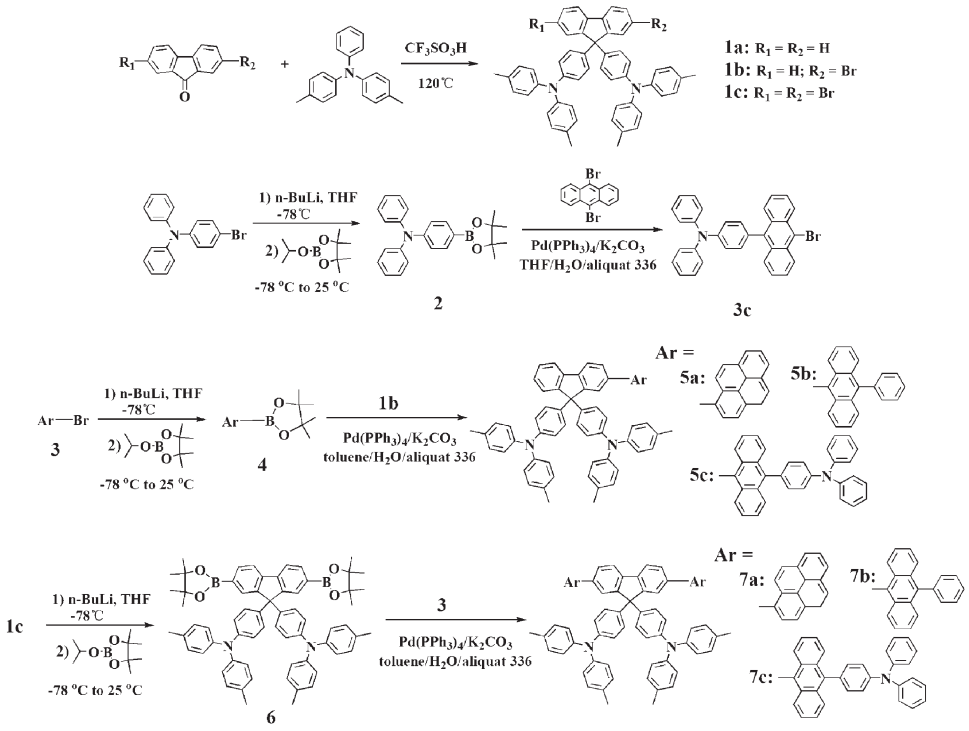

Scheme 1. Synthesis of the 9,9-di(4-(di-*p*-tolyl)aminophenyl)fluorene derivatives.

give the corresponding boronic esters **4a–c** with a yield of 33–57%. Then, Pd-catalyzed Suzuki coupling reactions between the boronic esters **4a–c** and the bromo compound **1b** were employed to introduce the bulky aryl groups into the C2 position of the fluorene molecules. The corresponding 2-arylfluorene derivatives **5a–c** were obtained in a 47–67% yield. The lithiation of **1c** with an excess amount of *n*-BuLi at −78 °C followed by treatment with 2-isopropoxy-4,4,5,5-tetramethyl-[1,3,2]dioxaborolane gave the diboronic esters **6**. The obtained diboronic esters **6** were treated with the bromides **3a–c**, respectively, to give the corresponding 2,7-diarylfluorene derivatives **7a–c** in modest yields (53–74%) by a Suzuki coupling reaction. The products **5a–c** and **7a–c** were purified by column chromatography on silica gel and/or vacuum sublimation. Pyrene, 10-phenylanthracene-9-yl, and 10-(4′-diphenylaminophenyl)anthracene-9-yl groups were introduced into the 2- and/or 7-positions of the fluorene ring because they are highly blue emissive and bulky, and thus are expected to improve the fluorescence quantum yield and thermal stability. Introducing 4,4′-dimethyltriphenylamine at the C9 position can further enhance the thermal stability of the fluorene derivatives.

2.2. Crystallographic Analyses

All of the the synthesized compounds were fully characterized with ^{1}H NMR spectroscopy, ^{13}C NMR spectroscopy, mass spectrometry (MS), and elemental analysis, and were found to be in good agreement with their structures. The crystal structures of **1a**, **5a**, **5c**, **7a**, and **7c** (Fig. 1 and **S1**) were further determined by X-ray structure analysis on single crystals, which were obtained by diffusion of hexane into their solutions in tetrahydrofuran or dichloromethane. Compounds **1a**, **5a**, **5c**, and **7a** crystallized in a triclinic system with a space group *P*–1, whereas **7c** crystallized in a monoclinic system with a space group *P*–121/n1 (see Table 1). Selected bond lengths, bond angles, and torsion angles are listed in Table 2. The five compounds contain almost-planar fluorene rings with torsion angles of C12–C11–C5–C6 less than |3.3| °. The substituents at the C2 position are highly twisted toward the fluorene backbone, and the torsion angles of

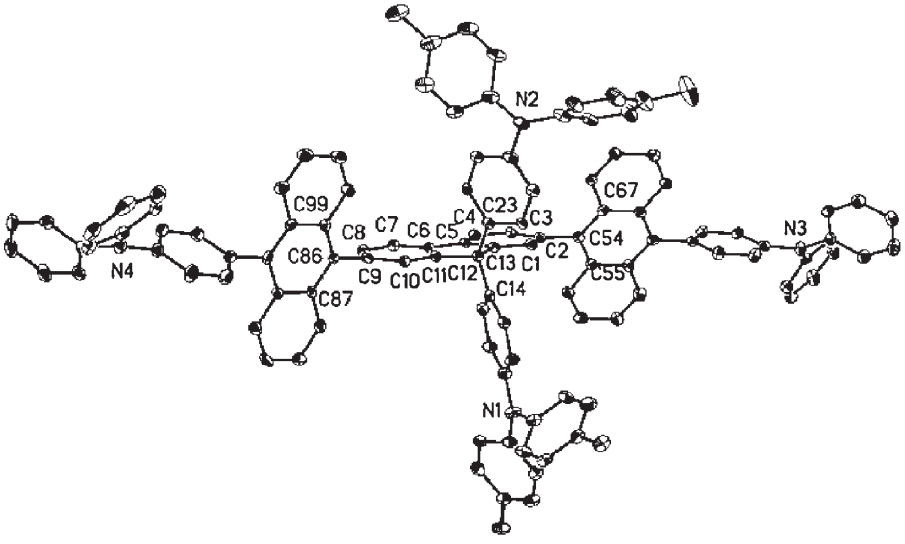

Figure 1. The crystal structure of compound **7c**. The solvent molecules have been omitted.

Table 1. Summary of crystal data for compounds **1a**, **5a**, **5c**, **7a**, and **7c**, including data collection and refinement details.

	1a	5a	5c	7a	7c
empirical formula	$C_{53}H_{44}N_2$	$C_{69}H_{52}N_2$	$C_{85}H_{65}N_3 \cdot CH_2Cl_2$	$C_{85}H_{60}N_2$	$C_{117}H_{84}N_4 \cdot 3CH_2Cl_2$
fw	708.90	909.13	1213.33	1109.35	1802.68
crystal system	triclinic	triclinic	triclinic	triclinic	monoclinic
space group	*P*–1	*P*–1	*P*–1	*P*–1	*P*–121/n1
A, [Å]	10.825(2)	13.5524(19)	13.855(6)	12.759(4)	15.4261(12)
b, [Å]	11.781(3)	14.254(2)	15.200(7)	13.614(4)	15.4261(12)
c, [Å]	17.237(4)	15.879(2)	18.423(7)	19.739(8)	20.3229(19)
α, [deg]	100.940(3)	79.788(12)	90.392(4)	82.434(18)	90
β, [deg]	99.540(2)	68.866(14)	90.605(7)	87.306(18)	97.722(4)
γ, [deg]	111.532(2)	73.368(12)	114.892(10)	61.099(11)	90
V, [Å^3]	1939.8(7)	2732.0(7)	3519(3)	2975.1(18)	10520.0(16)
Z	2	2	2	2	4
F(000)	752	960	1276	1168	3768
Crystal density (calcd), [mg/m^3]	1.214	1.105	1.145	1.238	1.138
μ, [mm^{-1}]	0.070	0.063	0.139	0.071	0.212
temp, [K]	113(2)	113(2)	113(2)	113(2)	113(2)
λ, [Å]	0.71070	0.71070	0.71070	0.71070	0.71070
2θ range, [deg]	1.93–27.87	1.38–25	1.62–25	1.72–25	1.57–25
Final *R* indices [$I > 2$sigma(I)]	$R_1 = 0.0488$	$R_1 = 0.0847$	$R_1 = 0.0824$	$R_1 = 0.0694$	$R_1 = 0.1307$
	$wR_2 = 0.1245$	$wR_2 = 0.2093$	$wR_2 = 0.2293$	$wR_2 = 0.1378$	$wR_2 = 0.3604$
R indices (all data)	$R_1 = 0.0730$	$R_1 = 0.1305$	$R_1 = 0.1318$	$R_1 = 0.1006$	$R_1 = 0.1675$
	$wR_2 = 0.1413$	$wR_2 = 0.2355$	$wR_2 = 0.2728$	$wR_2 = 0.1549$	$wR_2 = 0.3862$
Goodness-of-fit on $F^{\wedge 2}$	0.989	1.117	0.970	1.100	1.357

C8–C9–C54–C55 are −68.7° (**5a**) and 67.8° (**5c**), respectively. The two bulky triarylamines at the 9-position are nonplanar with the fluorine, with a C14–C12–C23 bond angle of 110–116°. This three-dimensionally non-coplanar conformation effectively releases the intermolecular interaction and inhibits self-aggregation and/or excimer formation in the solid state, reducing the chance of the unwanted long-wavelength emission.

Table 2. The selected bond lengths, bond angles, and torsion angles for the **1a**, **5a**, **5c**, **7a**, and **7c** Molecules.

structural parameter [a]	1a	5a	5c	7a	7c
C5–C6	1.464(2)	1.475(5)	1.464(5)	1.464(4)	1.473(6)
C6–C11	1.4002(19)	1.398(5)	1.392(5)	1.407(3)	1.406(7)
C11–C12	1.5351(18)	1.540(4)	1.560(5)	1.525(4)	1.535(7)
C12–C13	1.5319(18)	1.555(5)	1.547(5)	1.531(3)	1.545(6)
C13–C5	1.4016(19)	1.393(5)	1.404(5)	1.396(4)	1.406(7)
C12–C23	1.5391(18)	1.537(4)	1.527(5)	1.539(3)	1.543(6)
C12–C14	1.5349(17)	1.538(4)	1.535(5)	1.542(4)	1.541(7)
C9–C54		1.492(5)	1.511(5)	1.486(4) [b]	1.517(6) [c]
C2-C54				1.491(4)	1.502(7)
C5–C6–C11	108.79(12)	109.3(3)	109.7(3)	108.2(2)	107.9(4)
C6–C11–C12	110.62(12)	110.6(3)	109.7(3)	111.0(2)	112.1(4)
C11–C12–C13	101.08(10)	100.6(3)	100.6(3)	100.9(2)	99.9(4)
C12–C13–C5	110.63(12)	110.8(3)	110.1(3)	110.9(2)	111.2(4)
C13–C5–C6	108.84(12)	108.6(3)	109.0(3)	108.9(2)	108.8(4)
C14–C12–C23	111.29(11)	112.4(3)	112.9(3)	110.0(2)	115.5(4)
C11–C6–C5–C13	0.23(15)	0.8(4)	−0.7(4)	1.3(3)	−0.9(5)
C5–C6–C11–C12	0.95(14)	0.8(4)	3.3(3)	−3.3(3)	1.5(5)
C55–C54–C9–C10		−68.7(5)	67.8(5)	−54.1(4) [d]	76.5(6) [e]
C55–C54–C2–C1				62.9(3)	−63.8(6) [f]

[a] Bond angles and torsion ones are reported in degrees, and bond lengths in angstroms. [b] C9–C70. [c] C9–C86. [d] C83–C70–C2–C1. [e] C99–C86–C9–C10. [f] C67–C54–C2–C1.

2.3. Thermal Properties

The thermal properties of the six 2-monosubstituted and 2,7-disubstituted compounds were investigated by thermogravimetric analysis (TGA) and differential scanning calorimetry (DSC) (see Table 3). All of the compounds show glass-transition temperatures (T_g) higher than those obtained for the commonly used hole-transporting agents *N*,*N*′-diphenyl-*N*,*N*′-bis(3-methylphenyl)-1,1′-biphenyl-4,4′-diamine and 4,4′-bis(1-naphthylphenylamino)biphenyl. Introduction of the substituents into the 2-position of the fluorene is significantly beneficial to the morphological stability. The T_g value of the 2-monosubstituted compounds increases progressively on incorporating chromophores such as pyrene, 10-phenylanthracene-9-yl, and 10-triphenylaminoanthracene-9-yl groups. These substituents hinder close packing and intermolecular interaction, leading to the reduction of the crystallization tendency and to an increase in T_g. All of the materials show a distinct T_g of 153–174 °C. Furthermore, the six compounds show high thermal stabilities with decomposition temperatures (T_d) from 453–540 °C. Due to the thermal and morphological stability of the three compounds, homogeneous and stable amorphous thin films of the compounds could be prepared by vacuum deposition. Therefore, the introduction of the aryl substituents at the C2 and/or C7 positions is beneficial for

Table 3. Physical properties of the materials.

Compound	Yield	UV λ_{max}	Band gap	PL λ_{max}	$\eta_{solution}$	T_g	T_d	$E_{1/2}$	E_{HOMO}	E_{LUMO}
	[%]	[nm]	[eV]	[nm]	(%)	[°C]	[°C]	[eV]	[eV]	[eV]
1c	90	312	3.30	375	8		453	0.86	−5.16	−1.86
5a	67	360	2.97	460	60	153	453	0.88, 1.31	−5.18	−2.21
5b	59	382/403	2.84	440/453	77	159	487	0.88, 1.27	−5.18	−2.34
5c	47	385/401	2.77	468	61	166	509	0.85, 0.99, 1.25	−5.15	−2.38
7a	73	355	2.94	461	92	156	540	0.92, 1.35	−5.22	−2.28
7b	54	356	2.85	442	81		509	0.94, 1.33	−5.24	−2.39
7c	64	407	2.74	470	64	174	533	0.94, 1.30	−5.24	−2.50

improving the morphological stability and resistance to the thermal decomposition.

2.4. Optical and Photoluminescent Characteristics

Figure 2 shows the absorption and PL spectra of compounds **1a**, **5a–c**, and **7a–c** in toluene solution. Compounds **5a–c** and **7a–c** show a main absorption peak at 305–311 nm, which corresponds to the absorption of the model compound **1a**. In addition, the introduction of pyrene into the conjugated C2 and/or C7 positions of the fluorene leads to shoulder peaks at 345–370 nm corresponding to the $\pi \rightarrow \pi^*$ transition. In contrast to compounds **5a** and **7a**, compounds **5b**, **5c**, **7b**, and **7c** exhibit three absorption peaks at 356–400 nm with characteristic vibronic patterns, which are attributed to the $\pi \rightarrow \pi^*$ transition of anthracene. The C2-monosubstituted compounds in a dilute toluene solution exhibit absorption peaks similar to those of the C2,C7-disubsituted ones. Upon UV-light photoirradiation, the parent compound **1a**, unsubstituted at the C2 position, emits violet light at 370 nm. The compounds containing pyrene and 10-phenylanthracene-9-yl groups show a main emission peak at 405–428 nm accompanied by a shoulder peak at 415–447 nm, whereas the ones with 10-triphenylaminoanthracene-9-yl groups only exhibit an emission peak at 454 nm. The C2-aryl substituents have a pronounced effect on the PL spectra, which are red-shifted in the following order: pyrene, 10-phenylanthracene-9-yl, and 10-(4′-diphenylaminophenyl)-anthracene-9-yl groups. We observed that the C2,C7-disubstituted compounds exhibit emission peaks at a longer wavelength than those of the C2-monosubstituted ones. The fluorescent quantum yields (η_{PL}) of compounds **5a–c** and **7a–c** in toluene were measured to be 60–92% by using 9,10-diphenylanthracene as a standard, whereas the parent compound **1a** exhibits a low η_{PL} of 8%. Introduction of pyrene, 10-phenylanthracene-9-yl, and 10-(4′-diphenylaminophenyl)anthracene-9-yl groups into the C2 and/or C7 positions of the fluorene can substantially improve the fluorescent quantum yield because these substitutients are highly emissive. Therefore, aryl substituents at the C2- and/or C7 positions exhibit a pronounced effect on the absorption and PL spectra and the fluorescent quantum yields. The absorption spectra of the solution and film samples are almost identical (see Fig. 3), which implies a weak intermolecular interaction. In comparison with those in solution, the emission spectra of the thin films are obviously red-shifted due to the difference in the dielectric constant of the environment.[25] The **5a–c** and **7a–c** thin films show a blue emission with a peak at 440–470 nm without any tail in the longer-wavelength region, whereas the parent compound **1a**, unsubstituted at the C2 position, exhibits a violet-light emission at 374 nm with a tail in the visible region. Consequently, we suggest that the bulky pyrene, 10-phenylanthracene-9-yl, and 10-(4′-diphenylaminophenyl)anthracene-9-yl groups introduced into the C2 and/or C7 positions hinder the

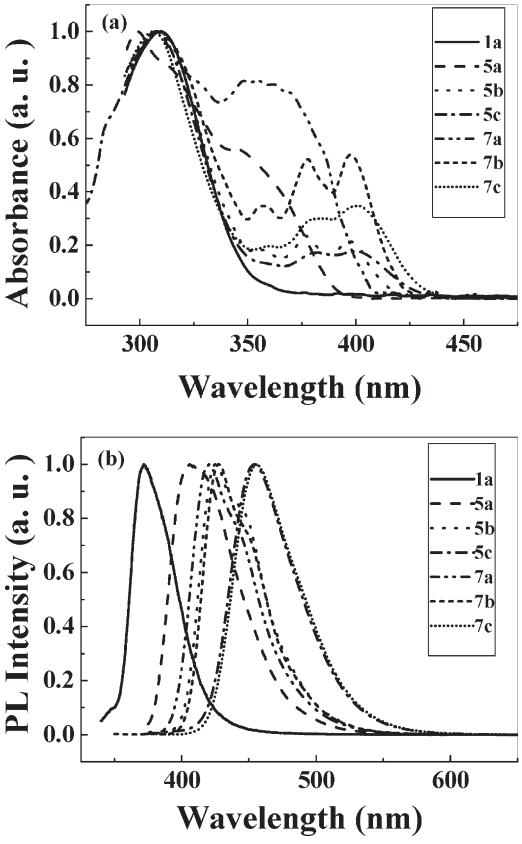

Figure 2. a) Absorption spectra and b) PL spectra of the compounds in toluene solution.

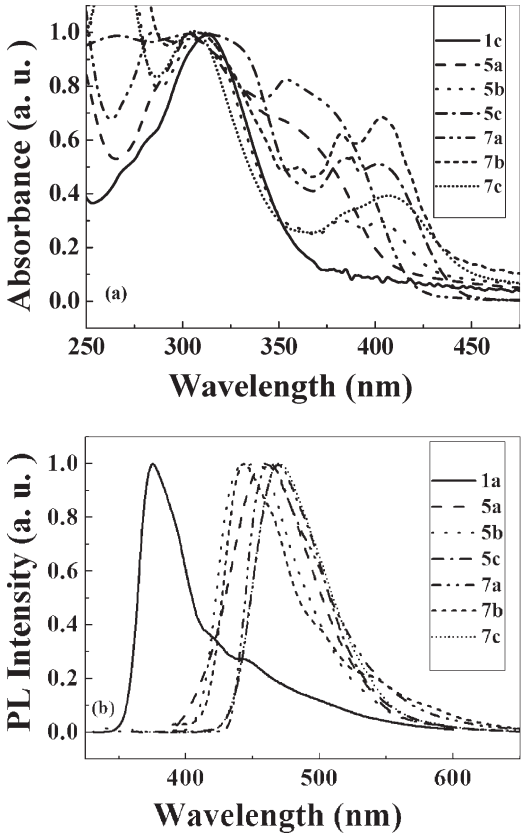

Figure 3. a) Absorption spectra and b) PL spectra of the compounds in the thin films.

formation of the excimer or molecular aggregation. To study the thermal stability of compounds **5a–c** and **7a–c**, the PL spectra of their thin films were recorded after a heating treatment in air and under ambient light. The annealed samples show PL spectra similar to those of the unannealed ones (**Fig. S2-S6**). Annealing did not result in long-wavelength emission and the color integrity remained after annealing at 130 °C for 24 h. Therefore, the PL spectra of compounds **5a–c** and **7a–c** have outstanding thermal stability, which could avoid the development of unwanted long-wavelength emission under device operation.

2.5. Molecular Orbitals, Excitation Energy, and Emission Energy

The photophysical characteristics of the organic materials depend mainly on their ground-and excited-state properties, which can be obtained via quantum chemical calculations. To explore the real origin of the photophysical properties, we optimized geometries of the ground (S_0) and excited-singlet (S_1) states of the fluorene derivatives, and calculated their absorption and emission wavelengths. The geometries of the S_0 and S_1 states were optimized by using B3LYP/6-31G* and CIS/3-21G*, respectively. The frontier molecular orbitals (FMOs) of the S_0 state for the all of the fluorene derivatives are shown in Figure 4 and **Figure S6-S12**. The HOMO, HOMO−1, and LUMO+3 of the parent compound **1a** are localized mainly on the two triarylamino groups at the 9-position of the fluorene, whereas the lowest unoccupied molecular orbital (LUMO) and HOMO−2 primarily arise from the fluorene. Moreover, the HOMO−3 and LUMO+2 of compound **1a** are localized predominantly on the fluorene and the two triarylamino groups, while the LUMO+1 is a combination of the fluorene and the two phenyl groups at the 9-position of the fluorene. Substituents at the 2- and/or 7-position of the fluorene have a remarkable influence on the FMOs of the S_0 states. The HOMOs of **5a** are localized mainly on one triphenylamino group at the 9-position of the fluorene, while the HOMO−1 is localized predominantly on another one. The LUMO and LUMO+2 of **5a** have similar molecular orbital (MO) distributions, which mainly arise from the pyrene. The HOMO−3, HOMO−2, and LUMO+1 of **5a** are distributed over the fluorene and pyrene, whereas the LUMO+3 is localized strongly on the fluorene and the two phenyl groups at the 9-position of the fluorene. Compounds **5b**, **5c**, and **7a** show HOMO and HOMO−1 distributions similar to those of compound **5a**. The HOMO−2 and LUMO of **5b** are localized predominantly on the anthracene, while the HOMO−3 and LUMO+1 primarily arise from the fluorene. The LUMO+2 of **5b** is distributed over the fluorene, anthracene, and two phenyl groups at the 9-position of the fluorene, whereas the LUMO+3 is localized predominantly on the anthracene, one phenyl ring at the fluorene, and the two phenyl groups at the 9-position. The HOMO−3 and LUMO of **5c** are localized strongly on the anthracene, while the HOMO−2 and LUMO+3 mainly arise from the triphenylamino group linking with the anthracene. The LUMO+1 of **5c** is

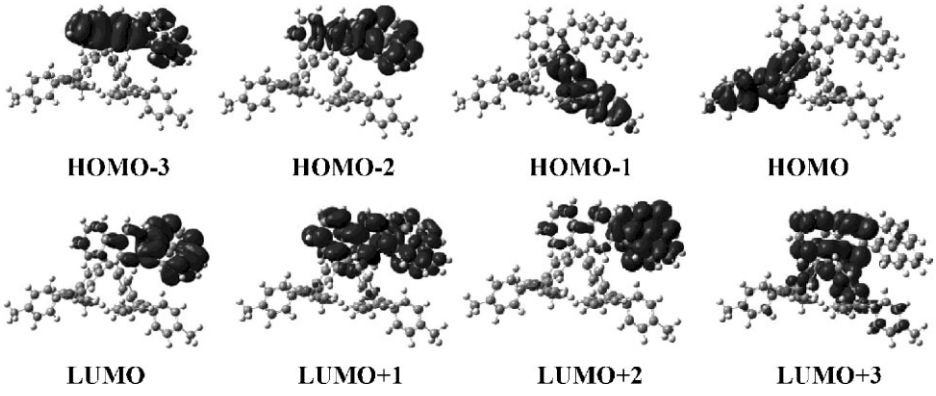

Figure 4. The frontier molecular orbitals of the S_0 state for compound **5a**.

ADVANCED FUNCTIONAL MATERIALS

localized primarily on the fluorene, whereas the LUMO+2 arises from the fluorene, anthracene, and the two phenyl groups at the 9-position of the fluorene. The HOMO−3, LUMO+1, and LUMO+3 of **7a** are localized mainly on the two anthracene groups, while the HOMO−2, LUMO, and LUMO+2 primarily arise from the two anthracenes and fluorene. The HOMO of **7a** is localized predominantly on one triphenylamino group at the 9-position of the fluorene, while the HOMO−1 is localized mainly on another triphenylamino group. The HOMO and HOMO−1 of **7b** are localized mainly on the two triphenylamino groups at the 9-position of the fluorene, whereas the HOMO−3, HOMO−2, and LUMO, and LUMO+1 arise from the two anthracenes. The LUMO+2 of **7b** is localized predominantly on the fluorene ring, while the LUMO+3 arises from the anthracene, fluorene, and two phenyl groups at the 9-position of the fluorene. Compound **7c** exhibits HOMO−1, HOMO, LUMO, and LUMO+1 distributions similar to those of **7b**. The HOMO−3 and HOMO−2 of **7c** are localized strongly on the two substituents at the 2,7-positions of the fluorene, while the LUMO+2 and LUMO+3 mainly arise from the fluorene. All of the seven compounds show almost the same HOMO energy levels because the HOMOs arise mainly from the triphenylamino groups at the 9-position.

Table 4 gives the calculated absorption wavelengths of the fluorene derivatives using TD-B3LYP with 6-31G* basis sets. For the seven fluorene derivatives, the absorption peak corresponding to the transition from the HOMO to the LUMO shows a very-low oscillator strength (f) of less than 0.01 due to their weak spatial overlap. Therefore, the above electronic transition could not result in the stronger optical absorption observed in the experiments. Frenking reported a similar result that the strong optical absorption for *mer*-Alq_3 does not arise from the transition from the HOMO to the LUMO.[26] The second longest absorption peak that was calculated has a larger f, being in better agreement with the experimental value in solution. The calculated absorption peak at 321 nm for the parent compound **1a** mainly results from the following transitions: HOMO → LUMO+3 (47%) and HOMO−1 → LUMO+1 (31%). For compounds **5a**, **5b**, and **7a**, we obtained a stronger absorption peak at 371, 397, and 394 nm, respectively, corresponding to the transition from HOMO−2 to LUMO. Compound **5c** exhibits a calculated absorption peak at 398 nm, resulting from the transition from HOMO−3 to LUMO. The calculated absorption peak at 398 nm for compound **7b** predominantly corresponds to the following transitions: HOMO−3 → LUMO+1 (42%) and HOMO−2 → LUMO (48%), while the one at 423 nm for compound **7c** mainly results from the HOMO−3 → LUMO+1 (47%) and HOMO−2 → LUMO (50%) transitions. **Figure S13** shows the change of the electron-density distribution upon the $S_0 \rightarrow S_n$ electronic transition of the fluorene derivatives. The calculated absorption peak at 321 nm for the parent compound **1a** mainly arises from the transition within the triphenylamino groups and the charge transfer from the triphenylamino groups to the fluorene ring. For compounds **5a** and **7a**, the absorptions at 371 or 394 nm predominantly result from the transition within the pyrene and one within the fluorene. The second longest absorption peak that was calculated for compounds **5b**, **5c**, and **7b** strongly correspond to the transition within

Table 4. Selected calculated excitation energies (E), wavelengths (λ), and oscillator strengths (f) for low-lying singlet (S_n) states of the fluorene derivatives.

Compound	State	Composition [a]	ΔE	λ	Experimental λ	f
			[eV]	[nm]	[nm]	
1a	S_1	H → L (70%)	3.52	353		0.01
	S_5	H → L+3 (47%)	3.86	321	309	0.40
		H−1 → L+1 (31%)				
5a	S_1	H → L (70%)	2.88	431		0.002
	S_3	H−2 → L (63%)	3.34	371	343–370	0.70
5b	S_1	H → L (70%)	2.76	449		0.001
	S_3	H−2 → L (64%)	3.13	397	396	0.20
5c	S_1	H → L (70%)	2.77	448		0.002
	S_4	H−3 → L (63%)	3.12	398	400	0.28
7a	S_1	H → L (70%)	2.76	449		0.01
	S_5	H−2 → L (67%)	3.14	394	343–370	0.97
7b	S_1	H → L (45%)	2.74	451		0.0001
		H−1 → L+1 (54%)				
	S_5	H−3 → L+1 (42%)	3.11	398	397	0.44
		H−2 → L (48%)				
7c	S_1	H → L (58%)	2.96	450		0.0
		H−1 → L+1 (41%)				
	S_5	H−3 → L+1 (47%)	2.93	423	400	0.19
		H−2 → L (50%)				

[a] H and L denote the HOMO and LUMO, respectively.

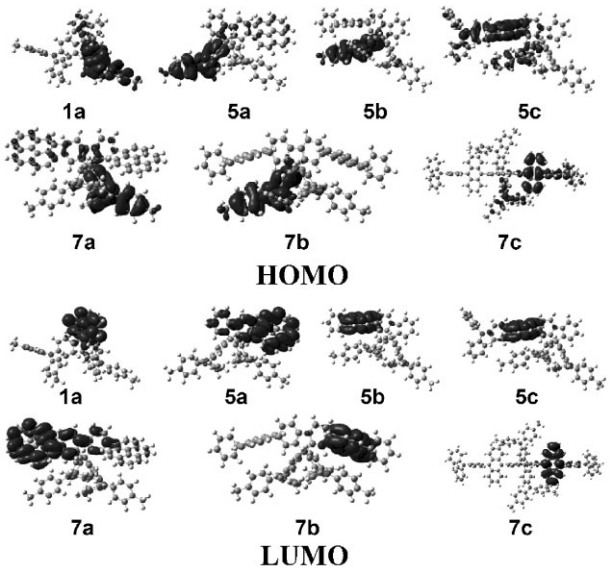

Figure 5. The HOMOs and LUMOs for the S_1 states of the fluorene derivatives.

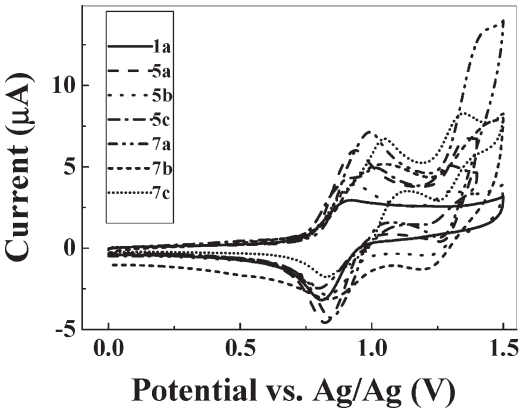

Figure 6. Cyclic voltammograms of compounds **1a**, **5a–c**, and **7a–c**.

anthracene, while that of **7c** mainly results from the transition within the substituents at the 2- and/or 7-position of the fluorene ring.

Figure 5 shows the HOMOs and LUMOs of the S_1 state for the fluorene derivatives. Compounds **1a**, **5a–b** and **7a–b** exhibit a similar HOMO distribution, which is localized mainly on one triphenylamino group at the 9-position of the fluorene. The HOMOs of compounds **5c** and **7c** are distributed predominantly over the anthracene, while they are localized to some extent on one triphenylamino group at the 9-position. We found that the LUMOs of **1a** primarily arise from the fluorene. The LUMOs of compounds **5a** and **7a** mainly lie on the pyrene groups and rarely result from the fluorene. The LUMOs of compounds **5b–c** and **7b–c** containing anthracene are localized predominantly on the anthracene. For compounds **1a**, **5a–c**, and **7a–c**, the calculated fluorescence emission wavelengths are predicted at 389, 468, 479, 478, 476, 479, and 479 nm, respectively. The electron transitions at these emission wavelengths correspond to the transitions from the LUMO to the HOMO. The calculated emission wavelengths can be compared with the experimental data in solution.

2.6. Electrochemical Peformance

Cyclic voltammetry (CV) measurements were carried out in a three-electrode cell setup with 0.1 M tetrabutylammonium hexafluorophosphate (Bu_4NPF_6) as a supporting electrolyte in anhydrous CH_2Cl_2 to probe the electrochemical behaviors of the materials. The electrochemical properties are shown in Figure 6 and Table 3. Compounds **5a**, **5b** and **7a–c** exhibit a similar electrochemical behavior. Two reversible anodic redox couples for the five compounds were obtained at 0.88–0.94 and 1.27–1.35 eV ($E_{1/2}$). However, compound **5c** shows three reversible anodic redox couples ($E_{1/2}$: 0.85, 0.99, and 1.25 eV). These results indicate that the first oxidation potentials are essentially unaffected by the substituents at the C2 and/or C7 positions of the fluorene due to the easy removal of electrons from the arylamino group at the C9 position. Both the onset potentials for oxidation and the first oxidation potentials of the six compounds are comparable to those of the model compound **1a**, indicating that the oxidation process of the compounds can be firstly delocalized on the triphenylamine at the C9 position. To assess the charge-injecting properties, the HOMO energy levels were estimated according to the equation: $E_{HOMO} = -([E_{1/2}]^{ox} + 4.3)$.[27] The six compounds show almost the same HOMO energy levels of about −5.20 eV, compared with that of the parent compound **1a** (−5.16 eV). This result indicates that the substituents at the C2 and/or C7 positions do not affect the hole-injecting characteristics and the HOMO energy levels depend mainly on the triphenylamino groups at the C9 positions. Such a high HOMO energy level greatly reduces the energy barrier for hole injection from indium tin oxide (ITO) ($\phi = 5.0$ eV) to the emissive fluorene derivatives. Most of the reported blue-light materials show a low HOMO energy level, leading to a difficult hole injection. The results presented suggest that the fluorene derivatives with the triphenylamino groups at the C9 positions can exhibit high HOMO energy levels, which allows effective hole injection. As a result, our compounds can also be used as hole-transport/injection materials. The LUMO energy levels for compounds **5a–c** and **7a–c** were determined to be −2.21, −2.34, −2.38, −2.28, −2.39, and −2.50 eV, respectively, by combining the HOMO energy levels together with the band gaps obtained from the absorption edge. Modification of the molecular structures has a significant effect on the electronic structure of the parent compound **1a**. Introducing the substituents into the C2 and/or C7 positions improves the π-conjugation effectively, reducing the LUMO energy level. Simultaneously, the extended π-conjugation also leads to a smaller energy gap.

ADVANCED FUNCTIONAL MATERIALS

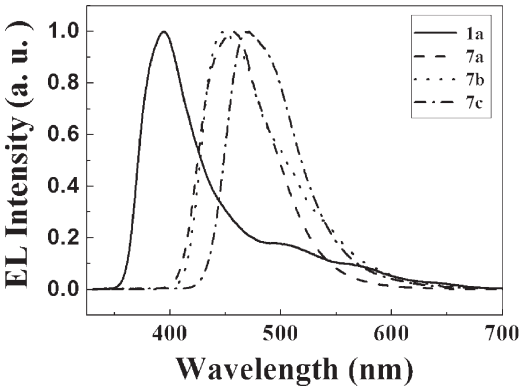

Figure 7. The EL spectra of compounds **1a** and **7a–c**.

2.7. Electroluminescent Properties

We fabricated OLEDs using compounds **7a–c** as the emissive layer with a structure of ITO/PEDT:PSS/fluorene derivative/TNS/Alq_3/LiF/Al, where the conducting polymer, polyethylene dioxythiophene:polystyrene sulfonate (PEDT:PSS); tetra(β-naphthyl)silane (TNS);[28] and tris(8-hydroxyquinolate) aluminum (Alq_3) were used as the hole-injection, hole-blocking, and electron-transporting layer, respectively. The combination of a thin LiF layer and Al has been shown to form an efficient cathode.[29] To compare, a device using the parent compound **1a** as the emissive layer was fabricated. The devices based on compounds **7a–c** show a blue-light emission with better CIE coordinates for **7a** (0.15, 0.16), **7b** (0.19, 0.22), and **7c** (0.15, 0.24). Figure 7 shows the EL spectra of OLEDs based on **7a–c** as the emissive layers. The similarity of the PL and EL spectra for the three compounds indicates that the EL is attributed to an emission from the corresponding emissive layer. We did not obtain tails in the longer-wavelength region of the EL spectra for compounds **7a–c**, which are often observed in the case of intermolecular π-stacking. This could result from the non-coplanar molecular structures of the materials, which hinder the formation of the excimer or molecular aggregation. We found that different applied voltages hardly affected the EL spectra of **7a–c** (see **Figure S14-S16**). Therefore, the EL spectra of compounds **7a–c** reveal excellent operating stabilities, which are consistent with the good thermal stabilities of their PL spectra. The key performance parameters of the devices are listed in Table 5. It is interesting to note that the device based on the blue compound **7c** exhibits a much-higher EL efficiency with a maximum current efficiency of 3.1 cd A^{-1} and external quantum efficiency of 1.8%, while the device efficiencies of the other two compounds are 1.3–1.75 cd A^{-1} with the same device configuration. The best EL characteristics, of compound **7c**, are attributed to the lowest LUMO energy level, leading to efficient injection of electrons from the electron-transporting layer into the emissive layer. High PL/EL quantum efficiencies, good carrier-transport properties, excellent spectral stabilities, and high HOMO energy levels render these compounds a very interesting and promising class of optoelectronic materials.

Table 5. The EL properties of the devices based on compounds **7a–c**.

Compound	λ_{EL}	CIE (x, y)	B_{max}	$\eta_{current}$	η_{ex}
	[nm]		[cd m^{-2}]	[cd A^{-1}]	[%]
7a	456	(0.15, 0.16)	1894	1.31	1.83
7b	448	(0.19, 0.22)	2227	1.75	1.10
7c	468	(0.15, 0.24)	2650	3.10	1.82

3. Conclusions

In summary, novel blue fluorene derivatives **5a–c** and **7a–c** containing bulky and highly blue-light emissive groups, as well as bulky hole-transporting ones, were designed and synthesized. These compounds have a three-dimensional conformation which is beneficial for inhibiting self-aggregation and/or excimer formation in the solid state. For the thin films of the fluorene derivatives, we obtained blue emission with a peak at 440–470 nm without an unwanted long-wavelength emission. Their PL spectra exhibit excellent thermal stability upon air annealing. Introducing triphenylamino groups into the C9 positions of the fluorene molecule results in suitable HOMO energy levels, which allows effective hole injection. Meanwhile, attachment of highly emissive groups, namely pyrene, 10-phenylanthracene-9-yl, and 10-(4′-diphenylaminophenyl) anthracene-9-yl groups, at the C2 and/or C9 positions increases the fluorescence quantum yield. The fluorene derivatives exhibit outstanding thermal stability with decomposition temperatures from 453 to 509 °C and show high glass-transition temperatures of 153–174 °C. Therefore, we can suggest that the successful synthesis of 2-aryl-9,9-di(triarylamino)fluorenes and 2,7-diaryl-9,9-di(triarylamino)fluorenes has opened the door to a novel class of blue-emitting materials with high fluorescence quantum yield and excellent thermal stability, as well as high HOMO energy levels. EL devices based on the synthesized fluorene derivatives produce bright-blue emission with a high EL efficiency of 3.1 cd A^{-1} (1.8%).

4. Experimental

Instrumentation: The ^{1}H NMR spectra were recorded using a Bruker DMX 300 NMR spectrometer; tetramethylsilane (TMS) was used as the internal standard. Mass spectrometry (MS) was performed on either an AEI-MS50-MS spectrometer, for electron impact MS (EI-MS) or a Bruker BIFLEXØ spectrometer for matrix-assisted laser desorption ionization with time-of-flight mode MS (MALDI-TOF-MS). Elemental analyses were obtained on a Carlo-Erba-1106 elemental analyzer. Thermogravimetric analysis (TGA) was carried out using a Perkin-Elmer thermogravimeter (Model TGA7) under a dry nitrogen gas flow at a heating rate of 20 °C min^{-1}. Glass-transition temperatures were determined by differential scanning calorimetry at a

heating rate of 20 °C min^{-1} using a Perkin-Elmer differential scanning calorimeter (DSC7). Crystal data were obtained with graphite-monochromated Cu K_α radiation ($\lambda = 0.71073$ Å) on a Rigaku RAPID IP imaging plate system. The structure was solved by direct method with the SHELXL97 program, and refined with full-matrix least-squares methods. Crystallographic data (excluding structure factors) for the structure(s) reported in this paper have been deposited with the Cambridge Crystallographic Data Centre as supplementary publication numbers CCDC 679040-679044.

Device Preparation: The organic EL devices were fabricated on a glass substrate coated with ITO (sheet resistance 30 Ω (square)$^{-1}$). A thin layer (30 nm) of poly(3,4-ethylenedioxythiophene):polystyrene sulfonic acid (PEDOT:PSS) was spin-coated onto the ITO as a hole injection layer. Then, a thin layer of the fluorene derivative (~50 nm) was spin-coated on top of the ITO/PEDOT:PSS surface as an emissive layer. Subsequently, TNS and Alq_3 organic layers were grown using thermal vacuum deposition in a vacuum of 2×10^{-4} Pa. The emitting area of the EL devices was 4 mm^2. Finally, a thin layer of electron-injection-facilitating LiF was introduced, followed by the deposition of 200 nm of aluminum as the cathode. A quartz-crystal oscillator placed near the substrate was used to measure the thickness of the thin films, which were calibrated ex situ using an Ambios Technology XP-2 surface profilometer. The absorption spectra of the thin films were studied using the quartz substrates.

Device Characterization: The absorption and photoluminescence spectra were measured with a General TU-1201 UV-vis spectrophotometer and a Hitachi F-4500 fluorescence spectrophotometer, respectively. The brightness and chromaticity coordinates were recorded with a Photo Research 650 spectrascan colorimeter. Current–voltage (*I–V*) characterisation was performed on a Hewlett-Packard 4140B semiconductor parameter analyzer. All of the measurements were performed under an ambient atmosphere at room temperature.

*Synthetic Procedures of the Compounds: 9,9-Di[4-(di-p-tolyl)aminophenyl]fluorene (**1a**)*: A mixture of fluorenone (2.16 g, 0.012 mol), 4,4′-dimethyltriphenylamine (15 g, 0.055 mol), and methanesulfonic acid (0.78 mL, 0.012 mol) was heated to about 120 °C under a nitrogen atmosphere until plenty of solid appeared and the stirring was stopped. The mixture was cooled down to room temperature and dissolved in chloroform. The solution was washed carefully with saturated $NaHCO_3$ solution, then with water and eventually dried over Na_2SO_4. After the solvent was partly removed under reduced pressure, acetone was added to give a pale-yellow precipitate. The solid was filtered and washed with acetone several times to give the pure product (11.0 g, 90.2%). MALDI-TOF-MS (*m/z*): [M^+] calcd for $C_{53}H_{44}N_2$, 708.35; found, 708.93; Anal. calcd for $C_{53}H_{44}N_2$: C 89.79, H 6.26, N 3.95; found: C 89.97, H 6.32, N 3.72.

*9,9-Di[4-(di-p-tolyl)aminophenyl]-2-bromofluorene (**1b**)*: A mixture of 2-bromofluorenone (3.1 g, 0.012 mol), 4,4′-dimethyltriphenylamine (15 g, 0.055 mol), and methanesulfonic acid (0.78 mL, 0.012 mol) was heated to about 120 °C under a nitrogen atmosphere until plenty of solid appeared and the stirring was stopped. The mixture was cooled down to room temperature and dissolved in chloroform. After removal of the solvent under reduced pressure, the residue was purified. The solution was then washed carefully with a saturated $NaHCO_3$ solution, then with water and eventually dried over Na_2SO_4. The solvent was partly removed and acetone was added to give a pale-yellow precipitate. The solid was filtered and washed with acetone several times to give a pure product (11.0 g, 90.2%). MALDI-TOF-MS (*m/z*): [M^+] calcd for $C_{53}H_{43}BrN_2$, 786.3; found, 786.7; Anal. calcd for $C_{53}H_{43}BrN_2$: C 80.80, H 5.50, N 3.56; found: C 80.65, H 5.64, N 3.54.

*9,9-Di[4-(di-p-tolyl)aminophenyl]-2,7-dibromofluorene (**1c**)*: A mixture of 2,7-dibromofluorenone (4.0 g, 0.012 mol), 4,4′-dimethyltriphenylamine (15 g, 0.055 mol), and methanesulfonic acid (0.78 mL, 0.012 mol) was heated to about 120 °C under a nitrogen atmosphere until plenty of solid appeared and the stirring was stopped. The mixture was cooled down to room temperature and dissolved in chloroform. After removal of the solvent under reduced pressure, the residue was purified, and the solution was washed carefully with a saturated $NaHCO_3$ solution, then with water and eventually dried over Na_2SO_4. The solvent was partly removed and acetone was added to give a pale-yellow precipitate. The solid was filtered and washed with acetone several times to give a pure product (8.7 g, 84%). ^{1}H NMR (300 MHz, $CDCl_3$, δ): 7.55 (d, 2H), 7.49–7.44 (t, 4H), 7.06–6.92 (m, 20H), 6.84 (d, 4H), 2.29 (s, 12H); ^{13}C NMR (400 MHz, THF-d_8, δ): 152.0, 145.3, 143.3, 136.3, 135.0, 130.6, 128.8, 127.8, 127.3, 126.6, 122.9, 119.9, 119.6, 119.4, 62.8, 18.0; MALDI-TOF-MS (*m/z*): [M^+] calcd for $C_{53}H_{42}Br_2N_2$, 864.2; found 864.9; Anal. calcd for $C_{53}H_{42}Br_2N_2$: C 73.45, H 4.88, N 3.23; found: C 73.39, H 4.86, N 3.28.

*4-(4,4,5,5-Tetramethyl-1,3,2-dioxaborolan-2-yl)triphenylamine (**2**)*: *n*-BuLi (4.8 mL, 12 mmol, 2.5 M solution in hexane) was added to a solution of 4-bromotriphenylamine (3.24 g, 10 mmol) in dry tetrahydrofuran (THF) (30 mL) at −78 °C under a nitrogen atmosphere. After the addition was complete, the reaction mixture was stirred for 1 h. 2-Isopropoxy-4,4,5,5-tetramethyl-1,3,2-dioxaborolane (2.45 mL, 12 mmol) was rapidly added to the mixture with constant stirring. The solution was heated slowly to room temperature and then stirred for another 12 h. After removal of the solvent under a reduced pressure, the residue was purified by column chromatography on a silica gel using a mixture of dichloromethane/petroleum ether (1:4) as the eluent. The product was obtained as a white solid in a 59% yield (2.2 g). ^{1}H NMR (300 MHz, DMSO-d_6, δ): 7.54 (d, 2H), 7.33 (t, 4H), 7.12–6.03 (m, 6H), 6.89 (d, 2H), 2.27 (s, 12H); ^{13}C NMR (300 MHz, $CDCl_3$, δ): 150.6, 147.4, 135.9, 129.4, 125.0, 123.4, 121.8, 83.6, 24.9; EIMS (*m/z*): [M^+] calcd for $C_{24}H_{26}BNO_2$, 371.2; found, 371); Anal. calcd for $C_{24}H_{26}BNO_2$: C 77.64, H 7.06, N 3.77; found: C 77.58, H 7.19, N 3.86.

*4-(10-Bromoanthracene-9-yl)triphenylamine (**3c**)*: Aqueous K_2CO_3 (2.0 M, 30 mL) and Aliquat 336 (80 mg) were added to a solution of 9,10-dibromoanthracene (5.04 g, 15 mmol) and **2** (1.86 g, 5 mmol) in THF (100 mL). After the mixture was degassed, tetrakis(triphenylphosphine)palladium ($Pd(PPh_3)_4$) (174 mg) was added in one portion under a nitrogen atmosphere. The reaction mixture was then heated and refluxed for 48 h under a nitrogen atmosphere. After it was cooled to room temperature, the solvent was evaporated under vacuum. The product was extracted with dichloromethane. The solution was washed with brine and H_2O, and then dried with $MgSO_4$. After removal of the solvent under reduced pressure, the crude product was purified by column chromatography on silica gel using petroleum ether as the eluent to offer a yellow-green solid in an 84% yield (2.1 g). ^{1}H NMR (300 MHz, DMSO-d_6, δ): 8.53 (d, 2H), 7.73 (t, 4H), 7.57 (t, 2H), 7.40 (t, 4H), 7.31 (d, 2H), 7.23–7.10 (m, 8H); ^{13}C NMR (400 MHz, $CDCl_3$, δ): 147.7, 147.4, 137.8, 132.0, 131.7, 131.3, 130.3, 129.5, 127.9, 127.5, 127.0, 125.5, 124.8, 123.3, 122.9, 122.6; MALDI-TOF-MS (*m/z*): [M^+] calcd for $C_{32}H_{22}BN$, 499.1; found, 499.4; Anal. calcd for $C_{32}H_{22}BrN$: C 76.80, H 4.43, N 2.80; found: C 76.82, H 4.48, N 3.12.

*1-(4,4,5,5-Tetramethyl-1,3,2-dioxaborolan-2-yl)-pyrene (**4a**)*: *n*-BuLi (2.4 mL, 6 mmol, 2.5 M solution in hexane) was added to a solution of 1-bromopyrene (**3a**) (1.41 g, 5 mmol) in 30 mL of tetrahydrofuran (THF) at −78 °C under a nitrogen atmosphere. After the addition was complete, the reaction mixture was stirred for 1 h. 2-Isopropoxy-4,4,5,5-tetramethyl-1,3,2-dioxaborolane (1.22 mL, 6 mmol) was rapidly added to the mixture with constant stirring. The solution was heated slowly to room temperature and then stirred for another 12 h. The solvents were removed under a reduced pressure. The crude product was purified by column chromatography on silica gel using a mixture of petroleum ether/dichloromethane (4:1) as the eluent to provide a yellow powder (0.55 g, 33.3%). ^{1}H NMR (300 MHz, $CDCl_3$, δ): 9.07 (d, 1H), 8.54 (d, 1H), 8.21–8.12 (m, 4H), 8.08–7.96 (m, 3H), 1.48 (s, 12H); ^{13}C NMR (300 MHz, $CDCl_3$, δ): 136.6, 134.0, 133.6, 131.2, 130.9, 128.6, 128.1, 127.9, 127.6, 125.8, 125.5, 125.3, 124.7, 124.5, 124.2, 84.0, 25.2; EIMS: (*m/z*): [M^+] calcd for $C_{22}H_{21}BO_2$, 328.2; found, 328; Anal. calcd for $C_{22}H_{21}BO_2$: C 80.51, H 6.45; found: C 80.31, H 6.62.

*9-(4,4,5,5-Tetramethyl-1,3,2-dioxaborolan-2-yl)-10-phenylanthracene (**4b**)*: *n*-BuLi (1.5 mL, 3.6 mmol, 2.5 M solution in hexane) was added to a solution of 9-bromo-10-phenylanthracene (**3b**) (1 g, 3 mmol)

ADVANCED FUNCTIONAL MATERIALS

in 30 mL of tetrahydrofuran (THF) at −78 °C under a nitrogen atmosphere. After the addition was complete, the reaction mixture was stirred for 1 h. 2-Isopropoxy-4,4,5,5-tetramethyl-1,3,2-dioxaborolane (0.74 mL, 3 mmol) was rapidly added to the mixture with constant stirring. The solution was heated slowly to room temperature and then stirred for another 12 h. The solvents were removed under a reduced pressure. The crude product was purified by column chromatography on silica gel using a mixture of petroleum ether as the eluent to provide a yellow powder (0.67 g, 58.5%). ^{1}H NMR (300 MHz, $CDCl_3$, δ): 8.45 (d, 2H), 7.63 (d, 2H), 7.57–7.52 (m, 3H), 7.47 (t, 2H), 7.40 (d, 2H), 7.31 (t, 2H), 1.60 (s, 12H); ^{13}C NMR (300 MHz, $CDCl_3$, δ): 139.8, 139.3, 135.6, 131.3, 129.9, 128.6, 128.5, 127.6, 125.6, 125.7, 125.1, 84.7, 25.4; EIMS (*m*/*z*): [M^+] calcd. for $C_{26}H_{25}BO_2$, 380.2; found, 380; Anal. calcd for $C_{26}H_{25}BO_2$: C 82.12, H 6.63; found: C 81.98, H 6.74.

*9-(4,4,5,5-Tetramethyl-1,3,2-dioxaborolan-2-yl)-10-(4-diphenylaminophenyl)anthracene (**4c**)*: *n*-BuLi (2.1 mL, 6 mmol, 2.5 M solution in hexane) was added to a solution of 4-(10-bromoanthracene-9-yl) triphenylamine (**3c**, 2.5 g, 5 mmol) in 100 mL of tetrahydrofuran (THF) at −78 °C under a nitrogen atmosphere. After the addition was complete, the reaction mixture was stirred for 1 h. 2-Isopropoxy-4,4,5,5-tetramethyl-1,3,2-dioxaborolane (1.22 mL, 6 mmol) was rapidly added to the mixture with constant stirring. The solution was heated slowly to room temperature and then stirred for another 12 h. The solvents were removed under a reduced pressure. The crude product was purified by column chromatography on silica gel using a mixture of petroleum ether as the eluent to provide a yellow powder (1.55 g, 56.5%). ^{1}H NMR (300 MHz, $CDCl_3$, δ) 8.45 (d, 2H), 7.78 (d, 2H), 7.52 (t, 2H), 7.44–7.34 (m, 6H), 7.30 (d, 3H), 7.24 (m, 3H), 7.18–7.09 (m, 4H), 1.60 (s, 12H); EIMS (*m*/*z*) [M^+] calcd for $C_{38}H_{34}BNO_2$, 547.3; found, 547.

*2-Pyrenyl-9,9-di(4-(di-p-tolyl)aminophenyl)fluorene (**5a**)*: 100 mL of toluene was added to a mixture of **1b** (1.887 g, 2.4 mmol) and **4a** (656 mg, 2 mmol). After 20 mL of 2 M aqueous potassium carbonate and Aliquat 336 (32 mg) were added to the mixture, the reaction solution was degassed under nitrogen atmosphere. Finally, 100 mg of $Pd(PPh_3)_4$ was added to the mixture. The reaction mixture was refluxed under flowing nitrogen for 36 h. After the reaction solution was cooled down to room temperature, the solvent was evaporated under a reduced pressure and the product was extracted with dichloromethane. The extraction solution was washed with brine and H_2O, and then was dried with anhydrous $MgSO_4$. The crude product was purified by column chromatography on silica gel using a mixture of dichloromethane/petroleum ether (1:9) as the eluent to provide a yellow-green solid in a 67.2% yield (1.22 g). ^{1}H NMR (300 MHz, $CDCl_3$, δ): 8.20 (t, 2H), 8.13–8.09 (m, 4H), 8.01 (d, 2H), 7.93 (d, 2H), 7.84 (d, 1H), 7.73 (s, 1H), 7.64 (d, 1H), 7.49 (d, 1H), 7.41 (t, 1H), 7.33 (t, 1H), 7.11 (d, 4H), 7.02–6.94 (m, 16H), 6.87 (d, 4H), 2.27 (s, 12H); MALDI-TOF-MS (*m*/*z*): [M^+] calcd for $C_{69}H_{52}N_2$, 908.4; found: 908.8; Anal. calcd. for $C_{69}H_{52}N_2$: C 91.15, H 5.76, N 3.08; found: C 90.69, H 5.74, N 3.44.

*2-(10-Phenylanthracene-9-yl)-9,9-di(4-(di-p-tolyl)aminophenyl)-fluorene (**5b**)*: **5b** was synthesized according to the procedure described for **5a** using **4b** (456 mg, 1.2 mmol), **1b** (1.13g, 1.44 mmol), 2.0 M K_2CO_3 (10 mL), $Pd(PPh_3)_4$ (70 mg), Aliquat 336 (20 mg), and toluene (80 mL). The crude product was purified by column chromatography on silica gel using a mixture of dichloromethane/petroleum ether (1:8) as the eluent to provide a yellow solid in a 59% yield (680 mg). ^{1}H NMR (300 MHz, $CDCl_3$, δ): 7.99–7.96 (m, 1H), 7.87 (d, 1H), 7.75–7.66 (m, 4H), 7.60–7.56 (m, 4H), 7.50–7.43 (m, 5H), 7.34–7.30 (m, 4H), 7.12 (d, 4H), 7.01 (d, 9H), 6.88 (d, 8H), 6.83 (d, 4H), 2.26 (s, 12H); MALDI-TOF-MS (*m*/*z*): [M^+] calcd for $C_{73}H_{56}N_2$, 960.4; found, 960.5; Anal. calcd for $C_{73}H_{56}N_2$: C 91.21, H 5.87, N 2.91; found: C 90.80, H 5.86, N 3.34.

*2-(10-(4′-Diphenylaminophenyl)anthracene-9-yl)-9,9-di(4-(di-p-tolyl) aminophenyl)fluorene (**5c**)*: **5c** was synthesized according to the procedure described for **5a** using **1b** (1.18 g, 1.5 mmol), **4c** (0.82 g, 1.5 mmol), 2.0 M K_2CO_3 (30 mL), $Pd(PPh_3)_4$ (70 mg), Aliquat 336 (25 mg), and THF (100 mL). The crude product was purified by column chromatography on silica gel using a mixture of petroleum ether as the eluent to provide a yellow solid in a 47.5% yield (790 mg). ^{1}H NMR (300 MHz, $CDCl_3$, δ): 7.96 (d, 1H), 7.85 (t, 3H), 7.73 (d, 2H), 7.55 (s, 1H), 7.52–7.447 (m, 2H), 7.445–7.25 (m, 18H), 7.08 (t, 6H), 7.99 (d, 8H), 6.91 (d, 8H), 6.84 (d, 4H), 2.26 (s, 12H); MALDI-TOF-MS (*m*/*z*): [$M^+ + 1$] calcd. for $C_{85}H_{65}N_3$, 1127.5; found, 1128.5; Anal. calcd for $C_{85}H_{65}N_3$: C 90.47, H 5.81, N 3.72; found: C 90.39, H 6.06, N 3.79.

*2,7-Di(4,4,5,5-tetramethyl-1,3,2-dioxaborolan-2-yl)-9,9-di(4-(di-p-tolyl)aminophenyl)fluorene (**6**)*: *n*-BuLi (6.72 mL, 16.8 mmol, 2.5 M solution in hexane) was added to a solution of **1c** (6.067 g, 7 mmol) in 20 mL of tetrahydrofuran (THF) at −78 °C under a nitrogen atmosphere. After the addition was complete, the reaction mixture was stirred for 1 h. 2-Isopropoxy-4,4,5,5-tetramethyl-1,3,2-dioxaborolane (3.43 mL, 16.8 mmol) was rapidly added to the mixture with constant stirring. The solution was heated slowly to room temperature and then was stirred for another 12 h. The solvents were removed under a reduced pressure. The crude product was purified by column chromatography on silica gel using a mixture of petroleum ether/dichloromethane (4:1) as the eluent to provide a white powder (1.7 g, 25%). ^{1}H NMR (300 MHz, $CDCl_3$, δ): 7.82 (d, 4H), 7.76 (d, 2H), 7.03 (t, 12H), 6.96 (d, 8H), 6.83 (d, 4H), 2.28 (s, 12H), 1.33 (s, 24H); MALDI-TOF-MS (*m*/*z*): [M^+] calcd for $C_{65}H_{66}B_2N_2O_4$, 960.5; found, 959.9; Anal. calcd for $C_{65}H_{66}B_2N_2O_4$: C 81.25, H 6.92, N 2.92; found: C 81.59, H 7.37, N 2.72.

*2,7-Dipyrenyl-9,9-di(4-(di-p-tolyl)aminophenyl)fluorene (**7a**)*: 50 mL of toluene was added to a mixture of **6** (478 mg, 1.7 mmol) and **3a** (672 mg, 0.7 mmol). After 5 mL of 2 M aqueous potassium carbonate and Aliquat 336 (11 mg) were added to the mixture, the reaction solution was degassed under a nitrogen atmosphere. Finally, 30 mg of $Pd(PPh_3)_4$ was added to the mixture. The reaction mixture was refluxed under flowing nitrogen for 36 h. After the reaction solution was cooled down to room temperature, the solvent was evaporated under a reduced pressure and the product was extracted with dichloromethane. The extraction solution was washed with brine and H_2O, and then was dried with anhydrous $MgSO_4$. The crude product was purified by column chromatography on silica gel using a mixture of dichloromethane/petroleum ether (1:4) as the eluent to provide a yellow solid in a 73% yield (570 mg). ^{1}H NMR (300 MHz, $CDCl_3$, δ): 8.24 (d, 2H), 8.20 (d, 4H), 8.15 (t, 2H), 8.08 (t, 6H), 8.02 (t, 4H), 7.96 (d, 2H), 7.80 (s, 2H), 7.71 (d, 2H), 7.23 (t, 4H), 7.02–6.95 (m, 16H), 6.92 (d, 4H), 2.26 (s, 12H); ^{13}C NMR (400 MHz, $CDCl_3$, δ): 152.3, 146.8, 145.4, 140.5, 139.0, 137.9, 132.3, 131.5, 131.0, 130.6, 130.0, 129.9, 128.93, 128.86, 128.5, 127.7, 127.5, 127.46, 126.0, 125.4, 125.2, 125.1, 125.0, 124.8, 124.7, 124.6, 122.4, 120.4, 64.8, 20.8; MALDI-TOF-MS (*m*/*z*): [M^+] calcd. for $C_{85}H_{60}N_2$, 1108.5; found, 1108.8; Anal. calcd for $C_{85}H_{60}N_2$: C 92.02, H 5.45, N 2.53; found: C 91.79, H 5.67, N 2.98.

*2,7-Di(10-phenylanthracene-9-yl)-9,9-di(4-(di-p-tolyl)aminophenyl) fluorene (**7b**)*: **7b** was synthesized according to the procedure described for **7a** using **6** (960 mg, 1 mmol), **3b** (766 mg, 2.3 mmol), 2.0 M K_2CO_3 (10 mL), $Pd(PPh_3)_4$ (70 mg), Aliquat 336 (16 mg), and toluene (50 mL). The crude product was purified by column chromatography on silica gel using a mixture of dichloromethane/petroleum ether (1:8) as the eluent to provide a yellow solid in a 54% yield (660 mg). ^{1}H NMR ($CDCl_3$, 300 MHz, δ): 8.10 (d, 2H), 7.80 (d, 4H), 7.69 (d, 4H), 7.62 (d, 10H), 7.47 (t, 4H), 7.34 (s, 8H), 7.20 (t, 4H), 6.96–6.85 (m, 20H), 2.25 (s, 12H); ^{13}C NMR (400 MHz, $CDCl_3$, δ): 152.5, 146.8, 145.4, 139.3, 139.2, 138.8, 137.34, 137.28, 132.1, 131.4, 130.9, 130.0, 129.98, 129.8, 128.5, 127.6, 127.1, 127.0, 125.2, 125.1, 124.3, 122.8, 120.3, 64.8, 20.8; MALDI-TOF-MS (*m*/*z*): [M^+] calcd. for $C_{93}H_{68}N_2$, 1212.5; found, 1212.4; Anal. calcd for $C_{93}H_{68}N_2$: C 92.04, H 5.65, N 2.31; found: C 91.68, H 5.46, N 2.44.

*2,7-Di(10-(4′-diphenylaminophenyl)anthracene-9-yl)-9,9-di(4-(di-p-tolyl)aminophenyl)fluorene (**7c**)*: **7c** was synthesized according to the procedure described for **7a** using **6** (769 mg, 0.8 mmol), **3c** (1g, 1.8 mmol), 2.0 M K_2CO_3 (30 mL), $Pd(PPh_3)_4$ (85 mg), Aliquat 336 (13 mg), and toluene (30 mL). The crude product was purified by

column chromatography on silica gel using a mixture of dichloromethane/petroleum ether (1:5) as the eluent to provide a yellow solid in a 64% yield (790 mg). ^{1}H NMR (300 MHz, $CDCl_3$, δ): 8.09 (d, 2H), 7.86 (d, 4H), 7.80 (d, 4H), 7.64 (s, 2H), 7.56 (d, 2H), 7.40 (t, 4H), 7.37–7.25 (m, 27H), 7.18 (d, 4H), 7.08 (t, 4H), 6.96 (d, 9H), 6.90 (d, 8H), 6.85 (d, 4H), 2.25 (s, 12H); ^{13}C NMR (400 MHz, $CDCl_3$, δ): 152.4, 147.8, 147.2, 146.6, 145.3, 139.2, 138.8, 138.3, 137.1, 137.08, 132.6, 132.1, 132.05, 130.8, 130.2, 130.0, 129.7, 129.4, 128.8, 127.1, 127.0, 125.1, 125.0, 124.7, 124.2, 123.1, 122.7, 120.2, 64.8, 20.8; MALDI-TOF-MS (m/z): [M^+] calcd. for $C_{117}H_{86}N_4$, 1546.7; found, 1548.0.

Received: January 16, 2008
Revised: March 5, 2008
Published online: July 18, 2008

[1] C. W. Tang, S. A. VanSlyke, *Appl. Phys. Lett.* **1987**, *51*, 913.

[2] a) F. C. Chen, Y. Yang, M. E. Thompson, J. Kido, *Appl. Phys. Lett.* **2002**, *80*, 2308. b) A. B. Tamayo, B. D. Alleyne, P. I. Djurovich, S. Lamansky, I. Tsyba, N. N. Ho, R. Bau, M. E. Thompson, *J. Am. Chem. Soc.* **2003**, *125*, 7377. c) Y. Shao, Y. Yang, *Appl. Phys. Lett.* **2003**, *83*, 2453. d) G. Yu, S. W. Yin, Y. Q. Liu, Z. G. Shuai, D. B. Zhu, *J. Am. Chem. Soc.* **2003**, *125*, 14816. e) Y. J. Shi, J. Liu, Y. Yang, *J. Appl. Phys.* **2000**, *87*, 4254. f) X. Gong, D. Moses, A. J. Heeger, S. Liu, A. K.-Y. Jen, *Appl. Phys. Lett.* **2003**, *83*, 183. g) J. Liu, Y. J. Shi, Y. Yang, *Appl. Phys. Lett.* **2001**, *79*, 578.

[3] a) Q. L. Huang, G. A. Evmenenko, P. Dutta, P. Lee, N. R. Armstrong, T. J. Marks, *J. Am. Chem. Soc.* **2005**, *127*, 10227. b) Y. Liu, M. Nishiura, Y. Wang, Z. M. Hou, *J. Am. Chem. Soc.* **2006**, *128*, 5592. c) J. Liu, T. F. Guo, Y. Yang, *J. Appl. Phys.* **2002**, *91*, 1595. d) R. J. Tseng, R. C. Chiechi, F. Wudl, Y. Yang, *Appl. Phys. Lett.* **2006**, *88*, 093512. e) C. T. Chen, Y. Wei, J. S. Lin, M. V. R. K. Moturu, W. S. Chao, Y. T. Tao, C. H. Chien, *J. Am. Chem. Soc.* **2006**, *128*, 10992.

[4] a) F. Huang, Y. H. Niu, Y. Zhang, J. W. Ka, M. S. Liu, A. K.-Y. Jen, *Adv. Mater.* **2007**, *19*, 2010. b) M. A. Baldo, D. F. O'Brien, Y. You, A. Shoustikov, S. Sibley, M. E. Thompson, S. R. Forrest, *Nature* **1998**, *395*, 151. c) Y. Wei, C. T. Chen, *J. Am. Chem. Soc.* **2007**, *129*, 7478. d) M. A. Baldo, M. E. Thompson, S. R. Forrest, *Nature* **2000**, *403*, 750. e) M. Sudhakar, P. I. Djurovich, T. E. Hogen-Esch, M. E. Thompson, *J. Am. Chem. Soc.* **2003**, *125*, 7796.

[5] a) J. X. Jiang, Y. H. Xu, W. Yang, R. Guan, Z. Q. Liu, H. Y. Zhen, Y. Cao, *Adv. Mater.* **2006**, *18*, 1769. b) J. Liu, Q. G. Zhou, Y. X. Cheng, Y. H. Geng, L. X. Wang, D. G. Ma, X. B. Jing, F. S. Wang, *Adv. Mater.* **2005**, *17*, 2914. c) X. Gong, S. Wang, D. Moses, G. C. Bazan, A. J. Heeger, *Adv. Mater.* **2005**, *17*, 2053. d) M. A. Baldo, S. Lamansky, P. E. Burrows, M. E. Thompson, S. R. Forrest, *Appl. Phys. Lett.* **1999**, *75*, 4. e) Y. Qiu, P. Wei, D. Q. Zhang, J. Qiao, L. Duan, L. K. Li, Y. D. Gao, L. D. Wang, *Adv. Mater.* **2006**, *18*, 1607.

[6] a) Q. F. Xu, H. M. Duong, F. Wudl, Y. Yang, *Appl. Phys. Lett.* **2004**, *85*, 3357. b) Y. Shao, Y. Yang, *Appl. Phys. Lett.* **2005**, *86*, 073510. c) H. Xia, M. Li, D. Lu, C. B. Zhang, W. J. Xie, X. D. Liu, B. Yang, Y. G. Ma, *Adv. Funct. Mater.* **2007**, *17*, 757.

[7] a) B. Carlson, G. D. Phelan, W. Kaminsky, L. Dalton, X. Z. Jiang, S. Liu, A. K.-Y. Jen, *J. Am. Chem. Soc.* **2002**, *124*, 14162. b) H. Tsuji, C. Mitsui, L. Llies, Y. Sato, E. J. Nakamura, *J. Am. Chem. Soc.* **2007**, *129*, 11902. c) J. H. Kim, M. S. Liu, A. K.-Y. Jen, B. Carlson, L. R. Dalton, C. F. Shu, R. Dodda, *Appl. Phys. Lett.* **2003**, *83*, 776. d) G. Zhou, M. Baumgarten, K. Müllen, *J. Am. Chem. Soc.* **2007**, *129*, 12211.

[8] a) C. Huang, C. G. Zhen, S. P. Su, K. Loh, Z. K. Chen, *Org. Lett.* **2005**, *7*, 391. b) K. Danel, T. H. Huang, J. T. Lin, Y. T. Tao, C. H. Chuen, *Chem. Mater.* **2002**, *14*, 3860. c) W. J. Shen, R. Dodda, C. C. Wu, F. I. Wu, T. H. Liu, H. H. Chen, C. F. Shu, *Chem. Mater.* **2004**, *16*, 930. d) C. J. Tonzola, A. P. Kulkarni, A. P. Gifford, W. Kaminsky, S. A. Jenekhe, *Adv. Funct. Mater.* **2007**, *17*, 863.

[9] a) M. F. Lin, L. Wang, W. K. Wong, K. W. Cheah, H. L. Tam, M. T. Lee, M. H. Ho, C. H. Chen, *Appl. Phys. Lett.* **2007**, *91*, 073517. b) Z. Q. Gao, B. X. Mi, C. H. Chen, K. W. Cheah, Y. K. Cheng, W. S. Wen, *Appl. Phys. Lett.* **2007**, *90*, 123506. c) H. Kanno, K. Ishikawa, Y. Nishio, A. Endo, C. Adachi, K. Shibata, *Appl. Phys. Lett.* **2007**, *90*, 123509. d) R. Meerheim, K. Walzer, M. Pfeiffer, K. Leo, *Appl. Phys. Lett.* **2006**, *89*, 061111. e) K. Walzer, B. Maennig, M. Pfeiffer, K. Leo, *Chem. Rev.* **2007**, *107*, 1233.

[10] X. J. Xu, S. Y. Chen, G. Yu, C. A. Di, Y. Q. Liu, *Adv. Mater.* **2007**, *19*, 1281.

[11] a) B. Domercq, C. Grasso, J. L. Maldonado, M. Halik, S. Barlow, S. R. Marder, B. Kippelen, *J. Phys. Chem. B* **2004**, *108*, 8647. b) D. D. Gebler, Y. Z. Wang, J. W. Blatchford, D. K. Jessen, S. W. Fu, T. M. Swager, A. G. MacDiarmid, A. J. Epstein, *Appl. Phys. Lett.* **1997**, *70*, 1644.

[12] a) A. Tsuboyama, H. Iwawaki, M. Furugori, T. Mukaide, J. Kamatani, S. Igawa, T. Moriyama, S. Miura, T. Kakiguchi, S. Okada, M. Hoshino, K. Ueno, *J. Am. Chem. Soc.* **2003**, *125*, 12971. b) J. Kido, Y. Okamoto, *Chem. Rev.* **2002**, *102*, 2357.

[13] a) K. T. Wong, Y. Y. Chien, R. T. Chen, C. F. Wang, Y. T. Lin, H. H. Chiang, P. Y. Hsieh, C. C. Wu, C. H. Chou, Y. O. Su, G. H. Lee, S. M. Peng, *J. Am. Chem. Soc.* **2002**, *124*, 11576. b) K. T. Wong, Z. J. Wang, Y. Y. Chien, C. L. Wang, *Org. Lett.* **2001**, *3*, 2285. c) M. C. Hung, J. L. Liao, S. A. Chen, S. H. Chen, A. C. Su, *J. Am. Chem. Soc.* **2005**, *127*, 14576. d) H. H. Lu, C. Y. Liu, C. H. Chang, S. A. Chen, *Adv. Mater.* **2007**, *19*, 2574.

[14] Y. H. Kim, D. C. Shin, S. S. Ko, C. H. Kim, H. S. Yu, Y. S. Chae, S. K. Kwon, *Adv. Mater.* **2001**, *13*, 1690. b) T. P. I. Saragi, T. Spehr, A. Siebert, T. Fuhrmann-Lieker, J. Salbeck, *Chem. Rev.* **2007**, *107*, 1011. c) A. P. Kulkarni, X. X. Kong, S. A. Jenekhe, *Macromelecules* **2006**, *39*, 8699. d) M. T. Bernius, M. Inbasekaran, J. O'Brien, W. S. Wu, *Adv. Mater.* **2000**, *12*, 1737.

[15] a) K. T. Wong, T. Y. Hwu, A. Balaiah, T. C. Chao, F. C. Fang, C. T. Lee, Y. C. Peng, *Org. Lett.* **2006**, *8*, 1415. b) C. C. Wu, Y. T. Lin, K. T. Wong, R. T. Chen, Y. Y. Chien, *Adv. Mater.* **2004**, *16*, 61. c) J. Luo, Y. Zhou, Z. Q. Niu, Q. F. Zhou, Y. G. Ma, J. Pei, *J. Am. Chem. Soc.* **2007**, *129*, 11314. d) C. Ego, A. C. Grimsdale, F. Uckert, G. Yu, G. Srdanov, K. Müllen, *Adv. Mater.* **2002**, *14*, 809.

[16] a) X. W. Chen, H. E. Tseng, J. L. Liao, S. A. Chen, *J. Phys. Chem. B* **2005**, *109*, 17496. b) K. Becker, J. M. Lupton, J. Feldmann, B. S. Nehls, F. Galbrecht, D. Q. Gao, U. Scherf, *Adv. Funct. Mater.* **2006**, *16*, 364. c) R. Grisorio, G. P. Suranna, P. Mastrorilli, C. F. Nobile, *Adv. Funct. Mater.* **2007**, *17*, 538. d) L. J. Rozanski, C. W. Cone, D. P. Ostrowski, D. A. V. Bout, *Macromolecules* **2007**, *40*, 4524. e) U. Scherf, E. J. W. List, *Adv. Mater.* **2002**, *14*, 477.

[17] E. J. W. List, R. Guentner, P. Scanducci de Freitas, U. Scherf, *Adv. Mater.* **2002**, *14*, 374.

[18] S. Y. Cho, A. C. Grimsdale, D. J. Jones, S. E. Watkins, A. B. Holmes, *J. Am. Chem. Soc.* **2007**, *129*, 11910.

[19] K. L. Chan, M. J. Mckiernan, C. R. Towns, A. B. Holmes, *J. Am. Chem. Soc.* **2005**, *127*, 7662.

[20] S. Setayesh, A. C. Grimsdale, T. Weil, V. Enkelmann, K. Müllen, F. Meghdadi, E. J. W. List, G. Leising, *J. Am. Chem. Soc.* **2001**, *123*, 946.

[21] Z. H. Li, M. S. Wong, H. Fukutani, Y. Tao, *Org. Lett.* **2006**, *8*, 4271.

[22] K. T. Wong, Z. J. Wang, Y. Y. Chien, C. L. Wang, *Org. Lett.* **2001**, *3*, 2285.

[23] a) X. J. Xu, G. Yu, C. A. Di, Y. Q. Liu, K. F. Shao, L. M. Yang, P. Lu, *Appl. Phys. Lett.* **2006**, *89*, 123503. b) K. F. Shao, Y. F. Li, L. M. Yang, X. J. Xu, G. Yu, Y. Q. Liu, *Chem. Lett.* **2005**, *34*, 1604.

ADVANCED FUNCTIONAL MATERIALS

[24] G. Yu, S. W. Yin, Y. Q. Liu, J. S. Chen, X. J. Xu, X. B. Sun, D. G. Ma, X. W. Zhan, Q. Peng, Z. G. Shuai, B. Z. Tang, D. B. Zhu, W. H. Fang, Y. Luo, *J. Am. Chem. Soc.* **2005**, *127*, 6335.
[25] L. Tao, Z. K. Peng, X. H. Zhang, P. F. Wang, C. C. Lee, S. T. Lee, *Adv. Mater.* **2005**, *15*, 1716.
[26] J. P. Zhang, G. Frenking, *J. Phys. Chem. A* **2004**, *108*, 10296.
[27] D. M. de Leeuw, M. M. J. Simenon, A. R. Brown, R. E. F. Einerhand, *Synth. Met.* **1997**, *87*, 53.
[28] G. Yu, X. J. Xu, Y. Q. Liu, Z. Q. Jiang, S. W. Yin, Z. G. Shuai, D. B. Zhu, X. B. Duan, P. Lu, *Appl. Phys. Lett.* **2005**, *87*, 222115.
[29] C. Adachi, T. Tsutsui, S. Saito, *Appl. Phys. Lett.* **1989**, *55*, 1489.